View metadata, citation and similar papers at core.ac.uk

brought to you by CORE

provided by Elsevier - Publisher Connector

Biochimica et Biophysica Acta 1828 (2013) 561–567

Contents lists available at SciVerse ScienceDirect

Biochimica et Biophysica Acta

journal homepage: www.elsevier.com/locate/bbamem

A lipid-dependent link between activity and oligomerization state of the *M. tuberculosis* SMR protein TBsmr

Karsten Mörs [a,b], Ute A. Hellmich [a,b], Daniel Basting [a,b], Philipp Marchand [a,b], Jan Philip Wurm [a,b], Winfried Haase [c], Clemens Glaubitz [a,b,*]

[a] Institute for Biophysical Chemistry, J.W. Goethe University, Frankfurt, Germany
[b] Centre for Biomolecular Magnetic Resonance, J.W. Goethe University, Frankfurt, Germany
[c] Max Planck Institute of Biophysics, Frankfurt, Germany

ARTICLE INFO

Article history:
Received 23 May 2012
Received in revised form 4 October 2012
Accepted 19 October 2012
Available online 24 October 2012

Keywords:
SMR transporter
EmrE
Lipid
Freeze fracture EM
NMR
Fluorescence

ABSTRACT

TBsmr is a secondary active multidrug transporter from *Mycobacterium tuberculosis* that transports a plethora of compounds including antibiotics and fluorescent dyes. It belongs to the small multidrug resistance (SMR) superfamily and is structurally and functionally related to *E. coli* EmrE. Of particular importance is the link between protein function, oligomeric state and lipid composition. By freeze fracture EM, we found three different size distributions in three different lipid environments for TBsmr indicating different oligomeric states. The link of these states with protein activity has been probed by fluorescence spectroscopy revealing significant differences. The drug binding site has been probed further by ^{19}F-MAS NMR through chemical labeling of native cysteine residues showing a water accessible environment in agreement with the alternating access model.

© 2012 Elsevier B.V. All rights reserved.

1. Introduction

The secondary multidrug/proton antiporter *M. tuberculosis* TBsmr (previously mmr (Rv3065)) from the SMR superfamily consists of 107 amino acids and has a sequence homology to *E. coli* EmrE of about 43%. EmrE forms four transmembrane helices [1–5], thus constituting the smallest known multidrug transporter [6]. The sequences of SMR proteins are predominantly hydrophobic with few polar residues. A glutamic acid in helix 1 (E13 in TBsmr, E14 in EmrE) is the only membrane-embedded charged residue. It is highly conserved among all studied SMR proteins [7] and was shown to be essential for SMR protein activity [8,9]. SMR proteins are active as dimers consisting of two four-helix bundles [5,10], while their orientation is still being discussed [11,12]. Low resolution cryo-EM [13] and X-ray [14] as well as recent NMR data [15] have been obtained for EmrE and show an antiparallel structure. However, the oligomeric form in vivo is not conclusively determined and could very well be tetrameric [16–18].

SMR proteins transport a variety of hydrophobic substrates including antibiotics and fluorescent dyes [19,20]. TBsmr is one of the transporters conveying multidrug resistance to *M. tuberculosis* [21], which belongs to the clinically most challenging MDR organisms [22]. Drug transport might occur by an alternating access model [23,24] similar to what has been proposed for secondary active importers such as LacY or LeuT [25,26]. A fluorescence study on TBsmr [8] demonstrated an occluded ethidium bound state (also found in EmrE [27,28]) in agreement with the alternating access transport hypothesis according to which the protein undergoes exchange between different conformational states [4,15,29].

Typically, transport activities were determined in *E. coli* lipids while in DMPC, binding affinities have been measured. A comparative study on EmrE and TBsmr examined the transport rate for methylviologen as a function of the lipid headgroup composition [30,31].

Here, we probe the oligomerization state of TBsmr in different lipid preparations by freeze fracture electron microscopy (FF-EM). The protein's capability to bind substrate and to form an occluded state during transport in these preparations was probed by observing fluorescence quantum yield and anisotropy changes of the substrate ethidium. Solvent accessibility was probed by ^{19}F MAS NMR on a transport competent state. Both EM and solid state NMR are perfectly equipped to investigate membrane proteins in their native environment, the lipid bilayer.

2. Materials and methods

2.1. Materials

All chemicals were purchased from Applichem (Darmstadt, Germany) unless indicated otherwise. Lipids were purchased from Avanti Polar Lipids (Alabaster, AL, USA).

* Corresponding author at: Institute for Biophysical Chemistry, J. W. Goethe University, Max-von-Laue-Str. 9, 60438 Frankfurt, Germany. Tel.: +49 69 798 29927; fax: +49 69 798 29929.
E-mail address: glaubitz@em.uni-frankfurt.de (C. Glaubitz).

0005-2736/$ – see front matter © 2012 Elsevier B.V. All rights reserved.
http://dx.doi.org/10.1016/j.bbamem.2012.10.020

2.2. Cloning

Wild-type TBsmr with Myc-His Tag in pT7-7 was kindly provided by S. Schuldiner, Hebrew University of Jerusalem. The single site mutations were introduced by site-directed mutagenesis (Stratagene, Amsterdam, Netherlands) with the following forward and reverse primer, respectively: TBsmr W30A 5′-GGT TCA CTC GGT TGG CGC CCA CGG TGG-3′, 5′-CCA CCG TGG GCG CCA ACC GAG TGA ACC-3′. TBsmr W30A C35S 5′-GGC CCA CGG TGG GCT CTC TAG TGG GTT ATG GC-3′, 5′-GCC ATA ACC CAC TAG AGA GCC CAC CGT GGG CC-3′, TBsmr W30A C8S C35S (TBsmr W30A ΔCys) 5′-CCT ATA CCT CTT GTC CGC GAT CTT CGC GG-3′, 5′-CCG CGA AGA TCG CGG ACA AGA GGT ATA GG-3′.

2.3. Expression, purification, reconstitution

TBsmr was expressed and purified as described previously [8]. Reconstitution of TBsmr was done by mixing the eluted protein with lipid solubilized in DDM. For removal of detergent the protein solution was incubated o/n at room temperature with Bio-Beads (Carl Roth GmbH, Karlsruhe, Germany).

2.4. Fluorescence measurements

For the fluorescence measurements TBsmr was reconstituted in *E. coli*, DMPC and POPC lipids at a ratio of 400:1 mol/mol (The lipid to protein ratio was estimated to be between 100:1 and 300:1 for the freeze fracture images.). Transport of ethidium was measured via a coupled transport assay. In short: Bio-Beads were removed after reconstitution and proteoliposomes were fused with purple membrane patches containing bacteriorhodopsin (bR) isolated from *Halobacterium salinarium*. BR and ethidium are excited simultaneously at 545 nm via a Jasco FP-6500 fluorescence spectrometer (Jasco, Groß-Umstadt, Germany). Temperatures were kept constant at 25 °C using a thermostatic circulating water bath (Thermofisher, Schwerte, Germany). While bR establishes a proton gradient, TBsmr starts transporting ethidium across the membrane. The transport results in a fluorescence increase, which is recorded. To collapse the proton gradient 1 μM CCCP are added to the sample solution. A detailed description of the assay is given in [8,32].

Steady state fluorescence anisotropy was measured with the ethidium concentration (2 μM) kept constant, and analyzed using Origin 8.5 (OriginLab Corporation, Northampton, MA, USA) using a single site binding model.

Leakage of protons across the bilayer was tested using 1 μM 8-Hydroxypyrene-1,3,6-trisulfonic acid, trisodium salt (HPTS). HPTS was incorporated into liposomes by freeze thawing and subsequent dialyzing at pH 7 over night at 4 °C. The HPTS containing liposomes were added to a buffer of pH 9.4 and the fluorescence change was recorded via a Jasco FP-6500 fluorescence spectrometer (Jasco, Groß-Umstadt, Germany).

2.5. Freeze fracture electron microscopy

Proteoliposomes with a lipid to protein ratio of 75:1 mol/mol (*E. coli* and DMPC) or 50:1 (POPC) in sample holders were frozen in ethane cooled to −180 °C by liquid nitrogen. Fracturing at −120 °C and replication at a shadowing angle of 45° with platinum/carbon was performed with a BAF 060 freeze-fracturing unit from Bal-Tec Inc. (Principality of Lichtenstein). The fracture images were enlarged from a ×16k to ×25k primary magnification to a final magnification of ×116,800 to ×194,500 and digitized (1024×1024 pixels). Images were analyzed by measuring the diameters of the protein particles perpendicular to the direction of shadowing (Fig. S1).

2.6. Simulation of particle size distributions

Theoretical particle size distribution functions were calculated for four different oligomeric states of TBsmr, which were approximated by different ellipsoids (Fig. 2, Fig. S4). Their dimensions were estimated from EmrE 2D crystal data (PDB: 2I68) [33]. The protein particles are randomly oriented within the membrane plane and with respect to the direction of shadowing resulting in a distribution function, which depends on the particle's size and shape. The shape of the observed distribution function is also affected by measurement errors due to limited resolution, which is approximated by a Gaussian distribution. Theoretical distribution functions were calculated for 200.000 random orientations and plotted as histograms (Fig. 2). Different standard deviations and bin sizes were used. Simulations were carried using Mathematica 7.0 (Wolfram Research). Further details are provided as supplementary material (Fig. S4).

2.7. ^{19}F solid state NMR spectroscopy

TBsmr wt and mutants were labeled with 3-Bromo-1,1,1-trifluoroacetone (BTFA) as described previously [34]. All spectra were acquired on a Bruker Avance 600 (600.13 MHz for ^{1}H and 564.69 for ^{19}F) using a 4 mm MAS DVT probehead (Bruker, Karlsruhe, Germany) at 275 K and 10 kHz MAS frequency. Chemical shift was referenced to Trifluoroacetic acid at 0 ppm. A typical 90° pulse was 4 μs with 60 kHz proton decoupling. Topspin (Bruker, Karlsruhe, Germany) were used for data acquisition and processing. Line broadening used for processing was 25 Hz. BTFA chemical shift calibration was carried out by solving BTFA in various water-free organic solvents. Dielectric constants were taken from the Bruker Almanac [35]. The observed chemical shifts could be described empirically by a monoexponential function $\delta = A\exp -\varepsilon/\varepsilon_0 + y$ (Eq. (1)).

3. Results

TBsmr was heterologously expressed in *E. coli*, purified, solubilized and reconstituted in DMPC, POPC and *E. coli* lipids. The choice of these lipids was mainly determined by the achieved reconstitution efficiency. TBsmr in these sample preparations has been analyzed in terms of its oligomeric state and its activity as outlined below.

3.1. Oligomeric state of TBsmr

The resulting proteoliposomes were analyzed by freeze–fracture electron microscopy. Protein particles can be observed as elevations within the proteoliposome images. In all three cases, a homogeneous protein distribution with no aggregates but different particle sizes is observed (Fig. 1a).

In order to quantify particle diameters, a statistical analysis had to be carried out. For freeze fracture EM the proteoliposomes are frozen (cryofixed) and then split along the bilayer interface by fracturing. This results in half membranes with protruding proteins (particles). By unidirectional shadowing with platinum–carbon, a replica is formed, which is observed by electron microscopy. The diameter of the particles was measured perpendicular to the direction of shadowing (Fig. S1). The platinum–carbon coat was subtracted (3.8 nm) from the obtained values [36]. The resulting particle size distributions were plotted as frequency histograms [37]. A resolution of up to ±0.5 nm has been determined for freeze fracture micrographs of gold particles [38] but a bin size of 0.8–1.0 nm was necessary here in order to smooth gaps in the histogram caused by the width of individual pixels in the digitized images. The resulting particle size distributions shown in Fig. 1b reveal mean distances and distribution widths of TBsmr particles of approx. 3.5 and 2 nm for DMPC, 5 and 4 nm for POPC and 5.5 and 6 nm for *E. coli* lipids.

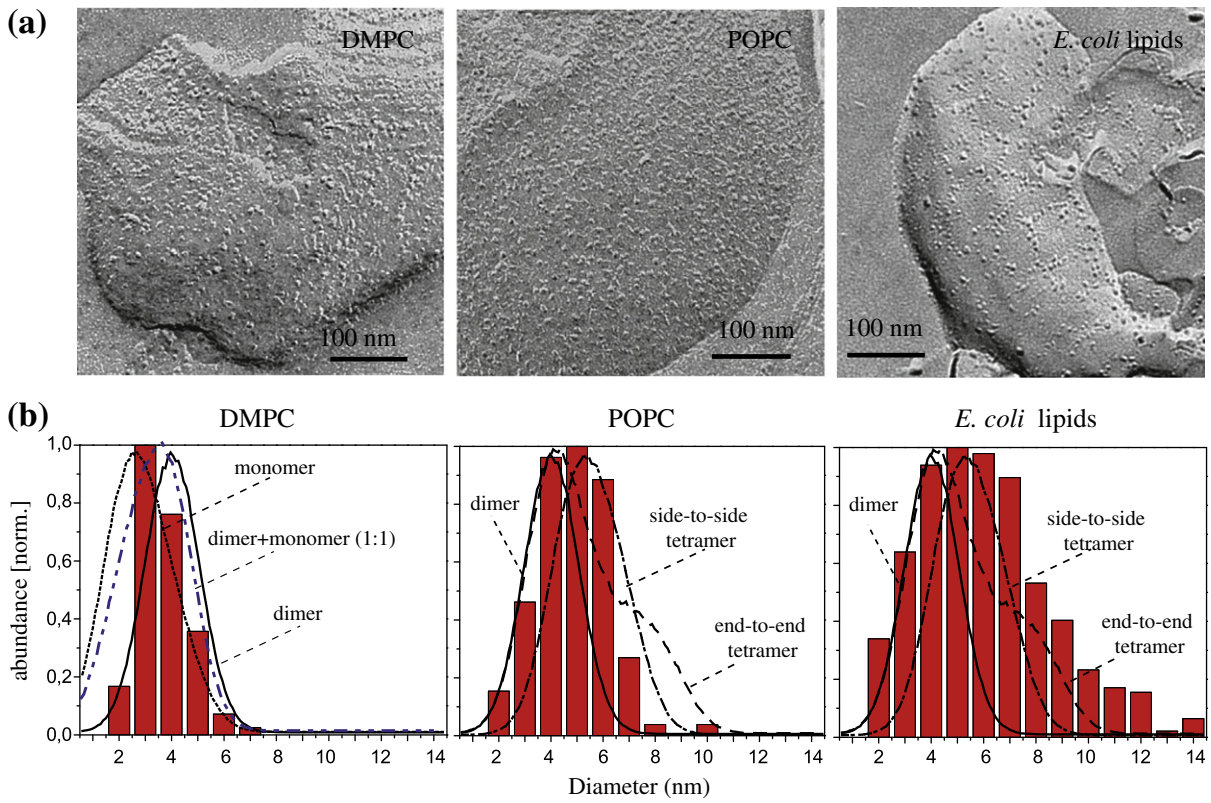

Fig. 1. (a) For each lipid an example freeze fracture electron microscopy image of reconstituted TBsmr is shown. A homogeneous distribution of the protein throughout the proteoliposomes is observed. (b) The distribution of particle diameters differs between all samples. The obtained particle size distributions are compared to those expected for a monomer, a dimer, a side-to-side tetramer and an end-to-end tetramer model (see Fig. 2). Between 100 and 300 particles were analyzed for each sample (0.8–1 nm bin size). The DMPC data can also be described by a superposition of monomer–dimer distribution functions indicating the existence of mixed populations.

It has been previously shown that the oligomeric state of a membrane protein can be estimated from its freeze fracture particle diameter [38]. We have therefore calculated particle size distributions, which would be expected for four different models. These models are based on the EM structure of EmrE (PDB: 2I68) [33] and biochemical data [5,18]. The size of a TBsmr dimer was estimated to be $3.1 \pm 0.1 \times 4 \pm 0.1$ nm. The possibility of a monomer and dimers of dimers was also included in the simulations. Possible arrangements of the tetramer are a side-to-side orientation with ~6.2×4 nm, as seen in the crystallographic tetramers of the EM structure [33], or an end-to-end tetramer (3.1×8 nm), based on the assumption that the oligomerization takes place at helix 4 [5,18]. Simulation results in Fig. 2 reveal a very broad distance distribution for an end-to-end tetramer but more narrow distributions functions for monomer, dimer and side-to-side tetramer. The latter distributions overlap significantly, but the dimer model shows a more narrow distribution with a smaller mean diameter. As expected, the monomer shows the smallest mean diameter, but its distribution width is comparable to the dimer model.

The calculated distribution functions and the experimental data are shown in Fig. 1b. Particle diameters and their distribution widths increase from DMPC to POPC and *E. coli* lipids. The experimentally observed particle size distribution in DMPC is not compatible with either tetrameric model and the center of the distribution is smaller than expected for a dimer but larger than expected for a monomer. In POPC, a particle size distribution comparable to dimer or side-to-side tetramer is observed. In *E. coli* lipids, a broad distribution is obtained. The overall shape of the distance distribution function can be reproduced by an end-to-end tetramer, but the high abundance of particles with larger diameters also indicates fractions of larger oligomers. The deviations of the experimental data from the assumed models are probably caused by the fact that the sample contains mixtures of monomers, dimers, both types of tetramers and higher oligomers. This is especially evident for the DMPC data, which can be also described by a superposition of monomer and dimer distribution functions (Fig. 1b, S5). Furthermore, the simulated particle size distributions are based on a simplified model and the limited number of particles detected could also restrict the experimental analysis.

3.2. Activity of reconstituted TBsmr

In order to test whether the oligomeric state observed in different lipid preparations correlates with transport activity of TBsmr, a fluorescence ethidium bromide (EtBr) assay as described in detail by Basting et al. [8] was carried out. Ethidium has been shown to be a substrate of multidrug transporters including EmrE and TBsmr [8,20,32,39]. In this assay, the proteoliposomes with reconstituted TBsmr are fused with purple membrane patches containing the proton pump bacteriorhodopsin (bR) [8,32]. Using a wavelength of 545 nm, bR and ethidium are excited simultaneously. bR starts pumping protons and builds up a proton gradient across the membrane, which is needed to drive substrate translocation. It was shown for EmrE and TBsmr that an occluded ethidium–protein complex is transiently formed in the presence of proton motif force [8,28]. In this situation, ethidium is excluded from water resulting in a significant increase of its fluorescence quantum yield observable at 610 nm. This unique possibility to observe a transient protein–substrate complex serves to assay activity of TBsmr.

It clearly can be observed that TBsmr is transport active in *E. coli* lipids as well as in POPC. Addition of carbonyl cyanide m-chlorophenyl hydrazone (CCCP), which uncouples the proton gradient, fully abolishes the formation of the fluorescent transport intermediate state. In DMPC, TBsmr displays no transport activity (Fig. 3a). The stability of the

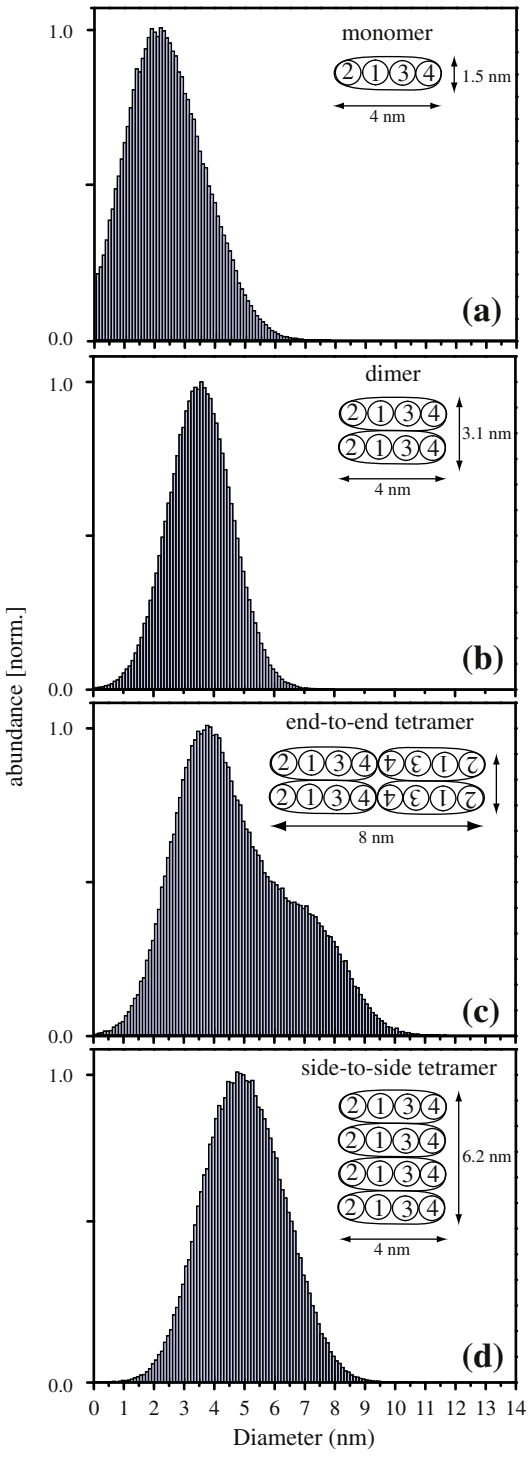

Fig. 2. Four theoretical particle size distributions were calculated assuming a TBsmr monomer (a), dimer (b), end-to-end tetramer (c) and side-to-side tetramer (d). The monomer and dimer shape was based on the EmrE crystal structure [33]. Histograms of 200,000 simulated elliptic particles with corresponding diameters (4.0×3.1 nm, 4.0×6.2 nm, 8.0×3.1 nm, respectively) with an allowed standard deviation of 1 nm per measurement were simulated. These simulations yield histograms (0.1 nm bin size) with a characteristic shape and width from which the oligomeric state of the particles can be estimated (see also Fig. S4). The side-to-side tetramer model was included for completeness but is less likely since such an inter-protein interface would lead to uncontrolled oligomerization [46].

generated pH gradient has been verified by control experiments using the pH sensitive dye HPTS trapped within the liposomes (Fig. S6a). In contrast to transport activity, equilibrium dissociation constants of ethidium, as determined by fluorescence anisotropy measurements, display similar values of about 1 μM for the three different lipid environments (Fig. 3b).

3.3. Probing the drug binding site of TBsmr

How substrates access the binding pocket of membrane proteins is difficult to answer generally. For EmrE it has been proposed that substrates can enter via the membrane and via a water filled pore [10]. Recent EPR data indicate water accessibility in proximity to the substrate binding site [40]. Our FF-EM data show that reconstitution of TBsmr in DMPC results in smaller particle sizes than in POPC and in *E. coli* lipids, while no transport activity is observed in DMPC. Particle size distributions are more homogeneous in POPC samples than in *E. coli* lipids. We have therefore probed the solvent accessibility of the drug binding site in TBsmr within POPC liposomes using ^{19}F solid state NMR. Our approach utilizes chemical labeling of accessible cysteines with 3-Bromo-1,1,1-trifluoroacetone (BTFA) attaching a trifluoromethyl group to the cysteine side-chain as described previously [34]. TBsmr contains two native cysteins C8 and C35 (Fig. S3). Residue C8 is in close proximity to the conserved residue E13 and could be utilized to probe the solvent accessibility of the drug binding pocket of TBsmr. ^{19}F chemical shifts of BTFA have been calibrated with respect to solvent polarity (Fig. 4b). To assign ^{19}F resonances, C35S and C8S/C35S mutations were introduced.

We found that expression yields were more consistent in our hands when an additional W30A mutation was introduced. TBsmr contains two tryptophan residues, W30 and W63, in its native sequence (Fig. S3). Only W63 is conserved in SMR proteins and relevant for drug transport [41]. Fluorescence transport and anisotropy measurements were carried out for all mutants TBsmr W30A, TBsmr W30A C35S and TBsmr W30A ΔCys and compared to wild-type TBsmr (Fig. S6b, S6c). Neither substrate binding nor transport was significantly affected by these mutations. This is not surprising because it has been shown for its homolog EmrE that mutations of most residues, including its native cysteines, do not impair transport ability [40,42,43].

TBsmr W30A and TBsmr W30A C35S were BTFA labeled and reconstituted into POPC liposomes. For both mutants, a broad ^{19}F resonance at a chemical shift of around −6 ppm was observed (Fig. 4a), while for TBsmr W30A, a second narrow signal at −4.9 ppm is detected. The resonances were fitted via a mixed Gauss–Lorentz line shape resulting in a peak ratio of approx. 20:1. As a control BTFA labeling was also applied to TBsmr W30A ΔCys resulting in no detectible NMR signal verifying specific labeling of accessible cysteines. It can therefore be concluded that the resonance at −6 ppm stems from labeled C8. The resonance observed at −4.9 ppm could originate from C35, but residual amounts of free label associated with the membrane could also contribute to this signal. We therefore restrict our data interpretation to C8. The BTFA chemical shift can be interpreted in terms of environmental polarity (Fig. 4b, Table S1). The ^{19}F chemical shift of C8 corresponds to a dielectricity constant close to water, which is in agreement with high water accessibility explaining the good labeling efficiency.

4. Discussion

Membrane protein function and structure are influenced by their respective lipid environment (e.g. [44]). Successful reconstitution, folding, the correct oligomerization state and activity of a membrane protein depend on the lipid composition of the bilayer it is inserted into. Here, we study the lipid dependent complex size of the MDR transporter TBsmr and correlate this with its transport activity and substrate binding capability. Furthermore, we can show that residues in the binding pocket of TBsmr are accessible to water, which is in agreement with current structural models [10,40].

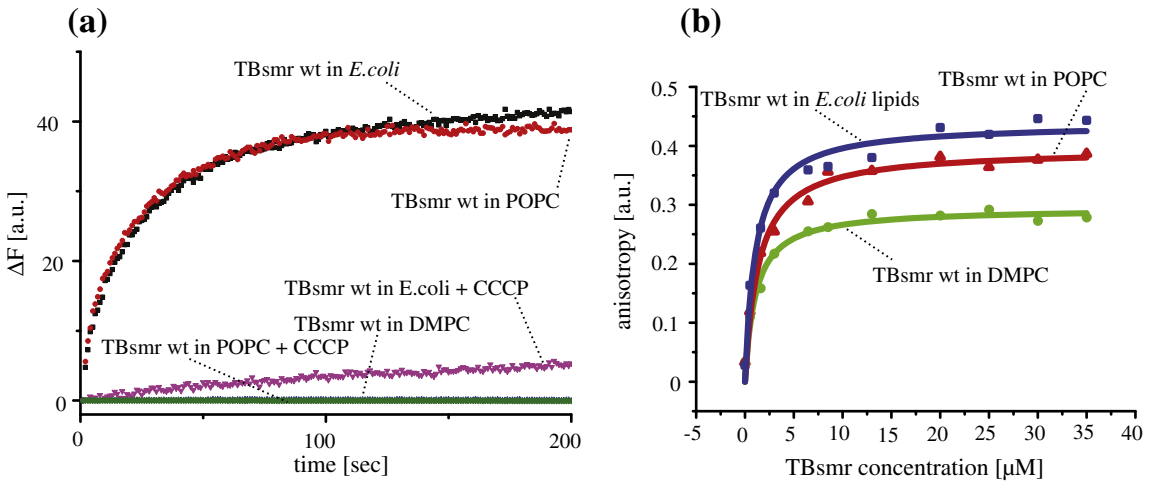

Fig. 3. (a) Transport of ethidium by TBsmr in DMPC, POPC and *E. coli* lipids has been assayed by fluorescence spectroscopy. The quantum yield of ethidium increases due to the formation of an occluded transport cycle intermediate state [8]. A stable transmembrane pH gradient is generated through illumination of TBsmr proteoliposomes fused with purple membrane patches. The relative activity of TBsmr is of the same magnitude in *E. coli* lipids and POPC. For TBsmr in DMPC no transport activity is observed. After addition of 1 μM CCCP, which collapses the ΔpH and ΔΨ, ethidium transport by TBsmr in all lipids is abolished. All measurements were carried out at a lipid to protein ratio of 400:1 (mol/mol). (b) Fluorescence anisotropy of ethidium in the presence of TBsmr DMPC, POPC and *E. coli* lipids was measured under equilibrium conditions, i.e. without a transmembrane pH gradient. The binding affinity of ethidium to TBsmr is around 1 μM in all three cases.

Freeze fracture EM shows very different TBsmr particle size distributions in different lipid environments (Fig. 1). In order to interpret our experimental data, we have calculated theoretical distributions for three oligomeric basic models (Fig. 2). The expected size distribution of the end-to-end tetramer model can be clearly distinguished from the dimer and the side-to-side tetramer. The latter two are less well distinguishable, but the dimer model shows a more narrow distribution with a smaller mean diameter. The experimentally observed particle size distribution in DMPC is not compatible with both tetrameric models but the center of the distribution is smaller than expected for a dimer and larger than a monomer. One possible reason could be a mixture between monomer and dimer populations (Fig. S4).

There is convincing evidence for dimer formation, e.g. from 2D crystallization in DMPC [33]. Such an end-to-end dimer would also agree well with crosslinking data on EmrE [16,45] and studies on the homolog SMR protein Hsmr [18], which show that transmembrane helix four is important for protein–protein interactions. Such interactions could drive the formation of dimers and end-to-end tetramers. These studies were carried out in *E. coli* lipids in which we have indeed observed particle size distributions compatible with a large fraction of end-to-end tetramers. The size distribution in POPC

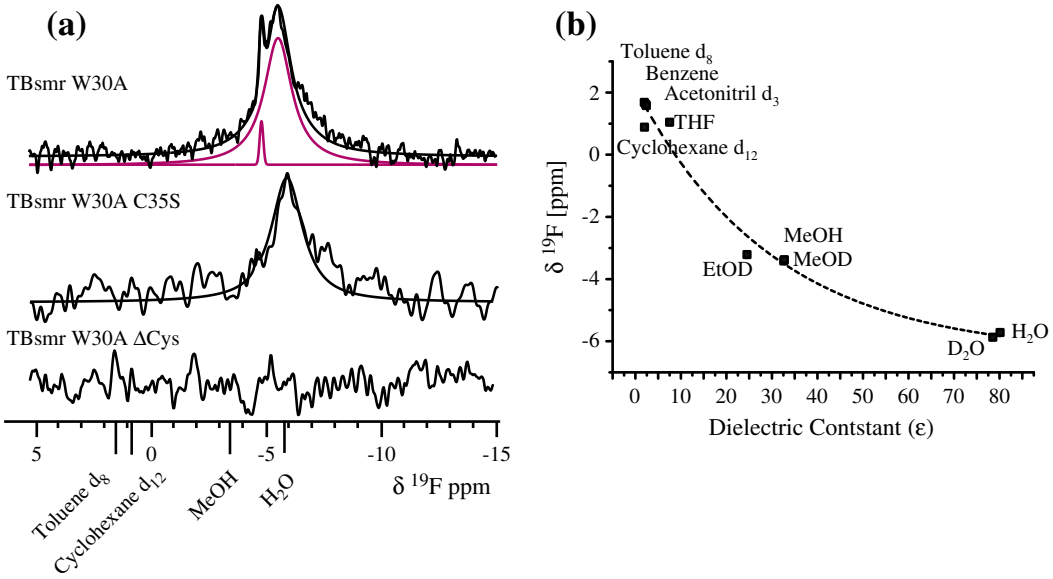

Fig. 4. (a) ^{19}F solid state NMR on BTFA labeled TBsmr mutants reconstituted in POPC. TBsmr W30A (top) contains both native cysteins C8 and C35. Labeling results in one major broad resonance at −6 ppm and a smaller narrow peak at −4.9 ppm. In TBsmr W30A C35S, only C8 can be labeled showing again a broad resonance at −6 ppm (middle). As a control, a cysteine free mutant TBsmr W30A C8S C35S was generated and subjected to the BTFA labeling procedure producing no detectable signal intensity (bottom). (b) The effect of environmental polarity onto the ^{19}F chemical shifts has been investigated by dissolving BTFA in various organic solvents with different dielectric constants ε within the range of 2 to 80 [35]. The chemical shift values can be described empirically as a function of ε by an exponential equation, allowing interpretation of experimentally observed chemical shifts of BTFA labeled residues in terms of water accessibility.

agrees with both dimer and side-to-side tetramer models. Both cases cannot be discriminated from each other within the resolution of the method and it is feasible that in POPC and *E. coli* lipids, TBsmr exists as mixture of dimers and higher oligomers. Nevertheless, a tetramerization interface involving all transmembrane helices and not just helix 4 could lead to uncontrolled oligomerization in the form of side-to-side tetramers [46] and is therefore unlikely (Fig. 2d).

The question arises whether protein activity is correlated with the observed particle size distribution. Indeed, we found that transport but not the binding properties of TBsmr seem to depend on the lipid environment. Unfortunately, substrate binding alone does not offer a strong criterion to assess a functional oligomeric state of an SMR protein. In case of EmrE for example, the K_d of ethidium was found to be similar for monomeric and dimeric preparations [47,48]. The observed K_d for ethidium binding to TBsmr is almost identical in all three lipid environments. This indicates similar binding pocket properties but no correlation between substrate binding and observable particle size distribution. In contrast to binding, ethidium transport clearly depends on the lipid environment and/or the observed particle size distribution. In both POPC and *E. coli* lipids, transport has been observed while TBsmr in DMPC did not show any transport capabilities. The lipid dependent activity of TBsmr could be either caused by a modulation of TBsmr's conformational equilibriums induced by bilayer properties or by specific protein–lipid interactions.

It has been shown before that TBsmr transport activity varies in different lipid mixtures by systematically varying their headgroups while keeping the chain lengths constant [31] but no data about the oligomeric state of TBsmr in these preparations exist. Our study suggests a link between lipid environment, complex formation and activity. Since time-consuming optimization of reconstitution conditions for FF-EM did not allow an extensive screen, we can only offer some educated guesses about the reasons for the observations reported here.

Both DMPC and POPC contain the same quaternary ammonium headgroup but vary in chain length and alkyl chain saturation (14:0 for DMPC, 16:0–18:1 for POPC). Variations of the alkyl chain length and of the degree of saturation modify thickness, order and lateral pressure profile of the membrane. It was for example reported that EmrE and TBsmr show decreasing transport activities with altered lateral pressure profiles [30,31], while Yeagle and colleagues demonstrated that transmembrane helix one of LacY alters its structural properties when presented with a hydrophobic mismatch [49]. Due to the shorter chain length of DMPC compared to POPC, such a mismatch might also occur for TBsmr and the resulting shift in its conformational equilibria might cause the protein's transport inactivity. This interpretation is also supported by our experiments in *E. coli* lipids: most lipid chains in *E. coli* membranes are in the range of 16 to 18 carbon atoms either without or with one double bond [50]. Why the observed particle size tends to be larger in *E. coli* lipids compared to POPC cannot be explained directly from our data. Both membranes differ in bilayer thickness, order and dynamics [51], which might modulate the conformational equilibriums of TBsmr in such a way that the formation of higher oligomers is promoted in *E. coli* while structural factors needed for transport are unaffected.

Our ^{19}F-MAS NMR data show that residue C8 is solvent exposed. C8 is located in helix 1 close to the highly conserved and functionally essential residue E13, which is responsible for drug binding and transport (Fig. S3). The observed water accessibility indicates a water accessible drug binding site in TBsmr reconstituted in POPC. This would be in agreement with the alternating access model as proposed previously [40,43,52]. This also correlates with recent EPR data on EmrE reconstituted in apolectin that show water accessibility along helix one and two [40]. Furthermore, cryo-EM data show that the EmrE drug binding pocket is accessible laterally from the bilayer and also via a water filled pore [10].

5. Conclusions

In summary, we find a correlation between TBsmr oligomerization and activity while a link between oligomerization and lipid environment seem to exist. In support of an alternating access model, we found water accessibility of residues close to the assumed drug binding/oligomerization interface. Further studies will include drug and pH titrations as well as a more comprehensive study of the effect of acyl chain length, headgroup and degree of saturation to investigate the oligomeric state and the drug/proton translocation pathway in more detail.

Abbreviations

bR	bacteriorhodposin
BTFA	3-bromo-1,1,1-trifluoroacetone
CCCP	carbonyl cyanide m-chlorophenyl hydrazone
DMPC	1,2-dimyristoyl-sn-glycero-3-phosphocholine
EtBr	ethidium bromide
FF-EM	freeze fracture electron microscopy
HPTS	8-hydroxypyrene-1,3,6-trisulfonic acid, trisodium salt
NMR	nuclear magnetic resonance
MDR	multi drug resistance
POPC	1-palmitoyl-2-oleoyl-sn-glycero-3-phosphocholine
SMR	small multidrug resistance protein
ssNMR	solid-state NMR

Acknowledgements

Shimon Schuldiner, Hebrew University of Jerusalem is acknowledged for providing plasmids used in this study. We would like to thank Gottfried Zimmermann for the help with acquiring data for Fig. 4, Jakob Lopez for the help with data evaluation and Ines Lehner, Camilo Perez and Christine Ziegler, Frankfurt for the helpful discussions. The work was funded through SFB 807 “Transport and communication across membranes”.

Appendix A. Supplementary data

Supplementary data to this article can be found online at http://dx.doi.org/10.1016/j.bbamem.2012.10.020.

References

[1] A.S. Purewal, Nucleotide sequence of the ethidium efflux gene from *Escherichia coli*, FEMS Microbiol. Lett. 82 (1991) 229–232.
[2] S. Schuldiner, EmrE, a model for studying evolution and mechanism of ion-coupled transporters, Biochim. Biophys. Acta, Proteins Proteomics 1794 (2009) 748–762.
[3] V.M. Korkhov, C.G. Tate, An emerging consensus for the structure of EmrE, Acta Crystallogr., Sect. D: Biol. Crystallogr. 65 (2009) 186–192.
[4] K. Henzler-Wildman, Analyzing conformational changes in the transport cycle of EmrE, Curr. Opin. Struct. Biol. 22 (2012) 38–43.
[5] S. Ninio, Y. Elbaz, S. Schuldiner, The membrane topology of EmrE — a small multidrug transporter from Escherichia coli, FEBS Lett. 562 (2004) 193–196.
[6] D. Bay, R. Turner, Diversity and evolution of the small multidrug resistance protein family, BMC Evol. Biol. 9 (2009) 140.
[7] S. Ninio, D. Rotem, S. Schuldiner, Functional analysis of novel multidrug transporters from human pathogens, J. Biol. Chem. 276 (2001) 48250–48256.
[8] D. Basting, M. Lorch, I. Lehner, C. Glaubitz, Transport cycle intermediate in small multidrug resistance protein is revealed by substrate fluorescence, FASEB J. 22 (2008) 365–373.
[9] H. Yerushalmi, S. Schuldiner, An essential glutamyl residue in EmrE, a multidrug antiporter from *Escherichia coli*, J. Biol. Chem. 275 (2000) 5264–5269.
[10] I. Ubarretxena-Belandia, C.G. Tate, New insights into the structure and oligomeric state of the bacterial multidrug transporter EmrE: an unusual asymmetric homo-dimer, FEBS Lett. 564 (2004) 234–238.
[11] P. Lloris-Garcera, F. Bianchi, J.S.G. Slusky, S. Seppala, D.O. Daley, G. von Heijne, Antiparallel dimers of the small multidrug resistance protein EmrE are more stable than parallel dimers, J. Biol. Chem. 287 (2012) 26052–26059.
[12] I. Nasie, S. Steiner-Mordoch, A. Gold, S. Schuldiner, Topologically random insertion of EmrE supports a pathway for evolution of inverted repeats in ion-coupled transporters, J. Biol. Chem. 285 (2010) 15234–15244.

[13] S.J. Fleishman, S.E. Harrington, A. Enosh, D. Halperin, C.G. Tate, N. Ben-Tal, Quasi-symmetry in the cryo-EM structure of EmrE provides the key to modeling its transmembrane domain, J. Mol. Biol. 364 (2006) 54–67.
[14] Y.-J. Chen, O. Pornillos, S. Lieu, C. Ma, A. Chen, G. Chang, X-ray structure of EmrE supports dual topology model, Proc. Natl. Acad. Sci. U.S.A. 104 (2007) 18999–19004.
[15] E.A. Morrison, G.T. DeKoster, S. Dutta, R. Vafabakhsh, M.W. Clarkson, A. Bahl, D. Kern, T. Ha, K.A. Henzler-Wildman, Antiparallel EmrE exports drugs by exchanging between asymmetric structures, Nature 481 (2012) 45–50.
[16] H. Yerushalmi, M. Lebendiker, S. Schuldiner, Negative dominance studies demonstrate the oligomeric structure of EmrE, a multidrug antiporter from *Escherichia coli*, J. Biol. Chem. 271 (1996) 31044–31048.
[17] C. Tate, I. Ubarretxena-Belandia, J. Baldwin, Conformational changes in the multidrug transporter EmrE associated with substrate binding, J. Mol. Biol. 332 (2003) 229–242.
[18] A. Rath, R.A. Melnyk, C.M. Deber, Evidence for assembly of small multidrug resistance proteins by a "two-faced" transmembrane helix, J. Biol. Chem. 281 (2006) 15546–15553.
[19] H. Yerushalmi, M. Lebendiker, S. Schuldiner, EmrE, an *Escherichia coli* 12-kDa multidrug transporter, exchanges toxic cations and H+ and is soluble in organic solvents, J. Biol. Chem. 270 (1995) 6856–6863.
[20] E. De Rossi, M. Branzoni, R. Cantoni, A. Milano, G. Riccardi, O. Ciferri, mmr, a *Mycobacterium tuberculosis* gene conferring resistance to small cationic dyes and inhibitors, J. Bacteriol. 180 (1998) 6068–6071.
[21] M. Balganesh, N. Dinesh, S. Sharma, S. Kuruppath, A.V. Nair, U. Sharma, Efflux pumps of *Mycobacterium tuberculosis* play a significant role in antituberculosis activity of potential drug candidates, Antimicrob. Agents Chemother. 56 (2012) 2643–2651.
[22] M. Alekshun, S. Levy, Molecular mechanisms of antibacterial multidrug resistance, Cell 128 (2007) 1037–1050.
[23] H.A. Koteiche, M.D. Reeves, H.S. Mchaourab, Structure of the substrate binding pocket of the multidrug transporter EmrE: site-directed spin labeling of transmembrane segment 1, Biochemistry 42 (2003) 6099–6105.
[24] M. Sharoni, S. Steiner-Mordoch, S. Schuldiner, Exploring the binding domain of EmrE, the smallest multidrug transporter, J. Biol. Chem. 280 (2005) 32849–32855.
[25] R. Kaback, R. Dunten, S. Frillingos, P. Venkatesan, I. Kwaw, W. Zhang, N. Ermolova, Site-directed alkylation and the alternating access model for LacY, Proc. Natl. Acad. Sci. U.S.A. 104 (2007) 491–494.
[26] L. Forrest, Y.-W. Zhang, M. Jacobs, J. Gesmonde, L. Xie, B. Honig, G. Rudnick, Mechanism for alternating access in neurotransmitter transporters, Proc. Natl. Acad. Sci. U.S.A. 105 (2008) 10338–10343.
[27] M. Lorch, S. Fahem, C. Kaiser, I. Weber, A.J. Mason, J.U. Bowie, C. Glaubitz, How to prepare membrane proteins for solid-state NMR: A case study on the alpha-helical integral membrane protein diacylglycerol kinase from E. coli, ChemBioChem 6 (2005) 1693–1700.
[28] I. Lehner, D. Basting, B. Meyer, W. Haase, T. Manolikas, C. Kaiser, M. Karas, C. Glaubitz, The key residue for substrate transport (Glu(14)) in the EmrE dimer is asymmetric, J. Biol. Chem. 283 (2008) 3281–3288.
[29] Y. Adam, N. Tayer, D. Rotem, G. Schreiber, S. Schuldiner, The fast release of sticky protons: kinetics of substrate binding and proton release in a multidrug transporter, Proc. Natl. Acad. Sci. U.S.A. 104 (2007) 17989–17994.
[30] P. Curnow, M. Lorch, K. Charalambous, P.J. Booth, The reconstitution and activity of the small multidrug transporter EmrE is modulated by non-bilayer lipid composition, J. Mol. Biol. 343 (2004) 213–222.
[31] K. Charalambous, D. Miller, P. Curnow, P. Booth, Lipid bilayer composition influences small multidrug transporters, BMC Biochem. 9 (2008) 31.
[32] M. Lorch, Lehner, A. Siarheyeva, D. Basting, N. Pfleger, T. Manolikas, C. Glaubitz, NMR and fluorescence spectroscopy approaches to secondary and primary active multidrug efflux pumps, Biochem. Soc. Trans. 33 (2005) 873–877.
[33] C.G. Tate, E.R. Kunji, M. Lebendiker, S. Schuldiner, The projection structure of EmrE, a proton-linked multidrug transporter from *Escherichia coli*, at 7 A resolution, EMBO J. 20 (2001) 77–81.
[34] U. Hellmich, N. Pfleger, C. Glaubitz, 19F-MAS NMR on proteorhodopsin: enhanced protocol for site-specific labeling for general application to membrane proteins, Photochem. Photobiol. 85 (2009) 535–539.
[35] Bruker, Almanac 2011 — Analytical Tables and Product Overview, Bruker, 2011.
[36] G.C. Ruben, J.N. Telford, Dimensions of active cytochrome c oxidase in reconstituted liposomes using a gold ball shadow width standard: a freeze-etch electron microscopy study, J. Microsc. 118 (1980) 191–216.
[37] U.W. Goodenough, L.A. Staehelin, Structural differentiation of stacked and unstacked chloroplast membranes. Freeze-etch electron microscopy of wild-type and mutant strains of *Chlamydomonas*, J. Cell Biol. 48 (1971) 594–619.
[38] S. Eskandari, E. Wright, M. Kreman, D. Starace, G. Zampighi, Structural analysis of cloned plasma membrane proteins by freeze–fracture electron microscopy, Proc. Natl. Acad. Sci. U.S.A. 95 (1998) 11235–11240.
[39] D. Bay, K. Rommens, R. Turner, Small multidrug resistance proteins: a multidrug transporter family that continues to grow, Biochim. Biophys. Acta, Biomembr. 1778 (2008) 1814–1838.
[40] S.T. Amadi, H.A. Koteiche, S. Mishra, H.S. McHaourab, Structure, dynamics and substrate-induced conformational changes of the multidrug transporter EmrE in liposomes, J. Biol. Chem. 285 (2010) 9.
[41] Y. Elbaz, N. Tayer, E. Steinfels, S. Steiner-Mordoch, S. Schuldiner, Substrate-induced tryptophan fluorescence changes in EmrE, the smallest ion-coupled multidrug transporter, Biochemistry 44 (2005) 7369–7377.
[42] M. Lebendiker, S. Schuldiner, Identification of residues in the translocation pathway of EmrE, a multidrug antiporter from *Escherichia coli*, J. Biol. Chem. 271 (1996) 21193–21199.
[43] S. Steiner-Mordoch, D. Granot, M. Lebendiker, S. Schuldiner, Scanning cysteine accessibility of EmrE, an H+-coupled multidrug transporter from *Escherichia coli*, reveals a hydrophobic pathway for solutes, J. Biol. Chem. 274 (1999) 19480–19486.
[44] J. Lundbaek, S. Collingwood, H. Ingolfsson, R. Kapoor, O. Andersen, Lipid bilayer regulation of membrane protein function: gramicidin channels as molecular force probes, J. R. Soc. Interface 7 (2009) 373–395.
[45] D. Rotem, N. Salman, S. Schuldiner, In vitro monomer swapping in EmrE, a multidrug transporter from *Escherichia coli*, reveals that the oligomer is the functional unit, J. Biol. Chem. 276 (2001) 48243–48249.
[46] A. Rath, C.M. Deber, Membrane protein assembly patterns reflect selection for non-proliferative structures, FEBS Lett. 581 (2007) 1335–1341.
[47] T.L. Winstone, M. Jidenko, M. le Maire, C. Ebel, K.A. Duncalf, R.J. Turner, Organic solvent extracted EmrE solubilized in dodecyl maltoside is monomeric and binds drug ligand, Biochem. Biophys. Res. Commun. 327 (2005) 437–445.
[48] C.W. Sikora, R.J. Turner, SMR proteins SugE and EmrE bind ligand with similar affinity and stoichiometry, Biochem. Biophys. Res. Commun. 335 (2005) 105–111.
[49] P. Yeagle, M. Bennett, V. Lemaitre, A. Watts, Transmembrane helices of membrane proteins may flex to satisfy hydrophobic mismatch, Biochim. Biophys. Acta, Biomembr. 1768 (2007) 530–537.
[50] S. Morein, A.-S. Andersson, L. Rilfors, G. Lindblom, Wild-type *Escherichia coli* cells regulate the membrane lipid composition in a "window" between gel and non-lamellar structures, J. Biol. Chem. 271 (1996) 6801–6809.
[51] R.S. Cantor, Lipid composition and the lateral pressure profile in bilayers, Biophys. J. 76 (1999) 2625–2639.
[52] I. Ubarretxena-Belandia, J.M. Joyce, C. Schuldiner, C.G. Tate, Three-dimensional structure of the bacterial multidrug transporter EmrE shows it is an asymmetric homodimer, EMBO J. 22 (2003) 6175–6181.